https://doi.org/10.5194/egusphere-2024-3170
Preprint. Discussion started: 22 November 2024

Benchmarking historical performance and future projections from a global hydrologic model with a basin-scale model

Rajesh R. Shrestha[1], Alex J. Cannon[1], Sydney Hoffman[2], Marie Whibley[2], Aranildo Lima[1]

[1]Climate Research Division, Environment and Climate Change Canada, Victoria, BC, Canada
[2]Watershed Hydrology and Ecology Research Division, Environment and Climate Change Canada, Victoria, BC, Canada

Correspondence to: Rajesh R. Shrestha (rajesh.shrestha@ec.gc.ca)

Abstract.

Global hydrologic models (GHMs) are increasingly relied upon for assessing climate-driven hydrologic changes from watershed to global scales. However, their ability to provide robust projections for a range of hydrologic variables remains unclear. Here, we evaluate the historical performance and future projections from the Community Water Model (CWatM) GHM against the Variable Infiltration Capacity (VIC) watershed hydrologic model for the Liard River basin in subarctic Canada. We drive both models with an ensemble of eight global climate models from the Coupled Model Intercomparison Project phase 6, downscaled and bias-corrected with a multivariate method. We analyze a range of hydrologic projections at 1.5 to 4.0 °C global warming levels (GWLs) above the preindustrial period. The historical performance benchmarking shows reasonable goodness-of-fit metrics for both models, with a slightly better performance for VIC. Projected hydrologic responses from CWatM are generally consistent with VIC in terms of annual water balance, and monthly snow water equivalent and flow changes, suggesting the robustness of the projections. Both models project coherent hydrologic changes, including progressively higher annual evapotranspiration; increased annual, winter, spring and maximum flows; increased frequency of extreme flow; and earlier timing of maximum flow, with higher GWLs. However, the magnitudes of maximum flow and late summer flow diverge between the two models, which can be explained by structural uncertainties associated with the representation of frozen soil and groundwater processes. Thus, our study provides insights into the robustness of hydrologic projections from a GHM, and offers a basis for model improvements.

https://doi.org/10.5194/egusphere-2024-3170
Preprint. Discussion started: 22 November 2024

1 Introduction

Hydrologic models are essential tools for assessing historical and future changes in water cycle variables from a watershed to regional and global scales. It is a common practice to employ watershed-scale hydrologic models for assessing the impacts of anthropogenically driven change, such as land use, riverine and climate change (e.g., Byun et al., 2019; Chegwidden et al., 2019; Eum et al., 2016; Shrestha et al., 2019). In recent years, global water models have increasingly been relied upon for assessing the past or present changes, and projecting future changes in hydrological variables from regional to global scales (e.g., Döll et al., 2018; Krysanova et al., 2020; Pokhrel et al., 2021; Greve et al., 2023).

Global water models broadly originate from the climate science community as land surface models, the global hydrology and water resources community as global hydrologic models, and the vegetation and carbon modelling community as dynamic vegetation models (Bierkens, 2015; Telteu et al., 2021). Particularly, global hydrologic models (GHMs) are closely related to watershed hydrologic models (WHMs) in terms of modelling philosophy and functionality but may differ with WHMs in physical process representation and spatial discretization. Specifically, GHMs are generally designed to provide consistent simulation of the water cycle components at continental or global scales with a simplified representation of physical processes (Hattermann et al., 2017; Veldkamp et al., 2018). In contrast, WHMs typically include more sophisticated and complex process representations that are often tailored to the specific characteristics of a watershed or river basin. In terms of spatial discretization, WHMs offer finer resolution (typically ≤ 10 km) than GHMs (typically 0.5° x 0.5° or ~50 km x 50 km at the equator), allowing for greater topographic complexity. The two modelling approaches may also differ in terms of model parameterization, with GHMs generally parameterized to represent large-scale processes and not calibrated to watershed-specific conditions, whereas WHM parameters are calibrated using river discharge and other available observations, e.g. snow water equivalent, evaporation etc. (Krysanova et al., 2020).

These differences could cause GHM-simulated responses to diverge from observations and WHM simulations, especially in replicating extreme maximum and minimum flows (Zaherpour et al., 2018; Heinicke et al., 2024). Additionally, all GHMs are not created equal, and differences in process representation can lead to substantial disagreements in simulated responses among models (Krysanova et al., 2020; Gnann et al., 2023). In northern regions, some GHMs may perform poorly due to the lack of representation of cold-climate processes (Gädeke et al., 2020).

These limitations are being addressed through ongoing enhancements in the GHMs (Bierkens, 2015; Telteu et al., 2021). For example, improvements in physical process representation have resulted in more reasonable reproduction of monthly and seasonal streamflow dynamics, as well as extreme flows (Huang et al., 2017; Veldkamp et al., 2018). Calibration of GHMs against observations (e.g. streamflow and evaporation) has also led to improvements in model performance (Zaherpour et al., 2018; Burek et al., 2020; Döll et al., 2024). Additionally, finer spatial resolutions of 5-arc minutes or less are becoming more common in GHMs (e.g., Burek et al., 2020; Hanasaki et al., 2022; van Jaarsveld et al., 2024). Thus, the predicted convergence of GHMs with WHMs (Bierkens, 2015; Bierkens et al., 2015) is being realized, and more consistent hydrological assessments from watershed to regional and global scales is being facilitated. There is, of course no guarantee that a model that performs well for the historical climate will provide reliable future projections (Krysanova et al., 2020). However, it could be argued that a GHM's ability to replicate future simulations of a WHM increases the confidence in GHM-based projections. In this respect, as suggested by Beven (2023) – a fit-for-purpose benchmarking to consider the suitability of a hydrologic model structure prior to a specific application – is highly relevant. Benchmarking GHMs prior to watershed scale or regional applications is also important

https://doi.org/10.5194/egusphere-2024-3170
Preprint. Discussion started: 22 November 2024

because these models are designed to represent large-scale hydrologic processes, and not tailored to specific hydrologic conditions.

Here, we present a benchmarking study that assesses the robustness of hydrologic responses from a GHM in comparison to a WHM in the context of climate change impacts. We focus on two key research questions: i) can a GHM, calibrated at a river basin scale, replicate the historical simulations and future projections from a WHM? ii) how do the model structural uncertainties affect the magnitude and direction of projected hydrologic response? To address these questions, we set up a state-of-the-art GHM, the Community Water Model (CWatM) (Burek et al., 2020) and a widely used WHM, the Variable Infiltration Capacity (VIC) (Liang et al., 1994; Hamman et al., 2018), for the Liard River basin in subarctic Canada. We drive both models with an ensemble of eight global climate models (GCMs) that participated in the Coupled Model Intercomparison Project phase 6 (CMIP6) experiment (Eyring et al., 2016), downscaled and bias-corrected with the MBCn multivariate bias correction algorithm (Cannon, 2018b). After benchmarking a set of statistical goodness-of-fit metrics of CWatM and VIC simulations, we analyze the robustness of a set of projected hydrologic responses, including annual water balance, monthly flow and snow water equivalent, annual maximum flow and timing, and flood frequencies. We compare the range, magnitude, and direction of changes, as well as the agreement between the model ensembles, at the 1.5, 2.0, 3.0 and 4.0 °C global warming levels above the preindustrial period. Furthermore, this study updates CMIP5 based VIC model projections for the Liard River basin from previous studies (Shrestha et al., 2019, 2022).

2. Study basin

This study focuses on the Liard River basin (LRB), a large mountainous basin in northwestern Canada with a drainage area of approximately 275,000 km^2. The river's headwaters originate in the Cordillera mountains, with the drainage area covering parts of four Canadian provinces/territories: Yukon, British Columbia, Northwest Territories and Alberta (Fig. 1). The Liard River is a major tributary of the Mackenzie River, covering about 16% of its drainage area and contributing about 25% of discharge (Shrestha et al., 2019). Located in the subarctic zone, most of the basin is underlain by discontinuous permafrost (based on the classification by Heginbottom et al. 1995). The LRB is mostly in a pristine state, with very limited resource development and about 74% forest coverage (Bonsal et al., 2020). Thus, the basin offers a good case for assessing the effects of GHM and WHM structures in simulating the cold-climate hydrologic regime, dominated by flows from snowmelt and frozen ground, and not affected by direct human impacts such as dams and reservoirs.

The mountainous topography of the region exerts a strong influence on the basin's climatology, particularly over the Cordillera mountains, creating a strong precipitation gradient (Szeto et al., 2008). The mean annual precipitation, temperature, and runoff in the basin over the years 1979-2012 were about 570 mm, -2.0 °C, and 290 mm, respectively (Shrestha et al., 2019). Seasonally, the basin receives a higher fraction of annual precipitation between April and September, while the runoff regime is dominated by snowmelt-driven high flows during spring and summer months (Woo and Thorne, 2006). Annual air temperature and precipitation in the basin have increased by 2.2 °C and 12%, respectively, over the years 1948-2016 (Bonsal et al., 2020). However, mean annual and maximum streamflow trends for most stations in the basin are negligible, except for the minimum flow increases (Shrestha et al., 2021).

https://doi.org/10.5194/egusphere-2024-3170
Preprint. Discussion started: 22 November 2024

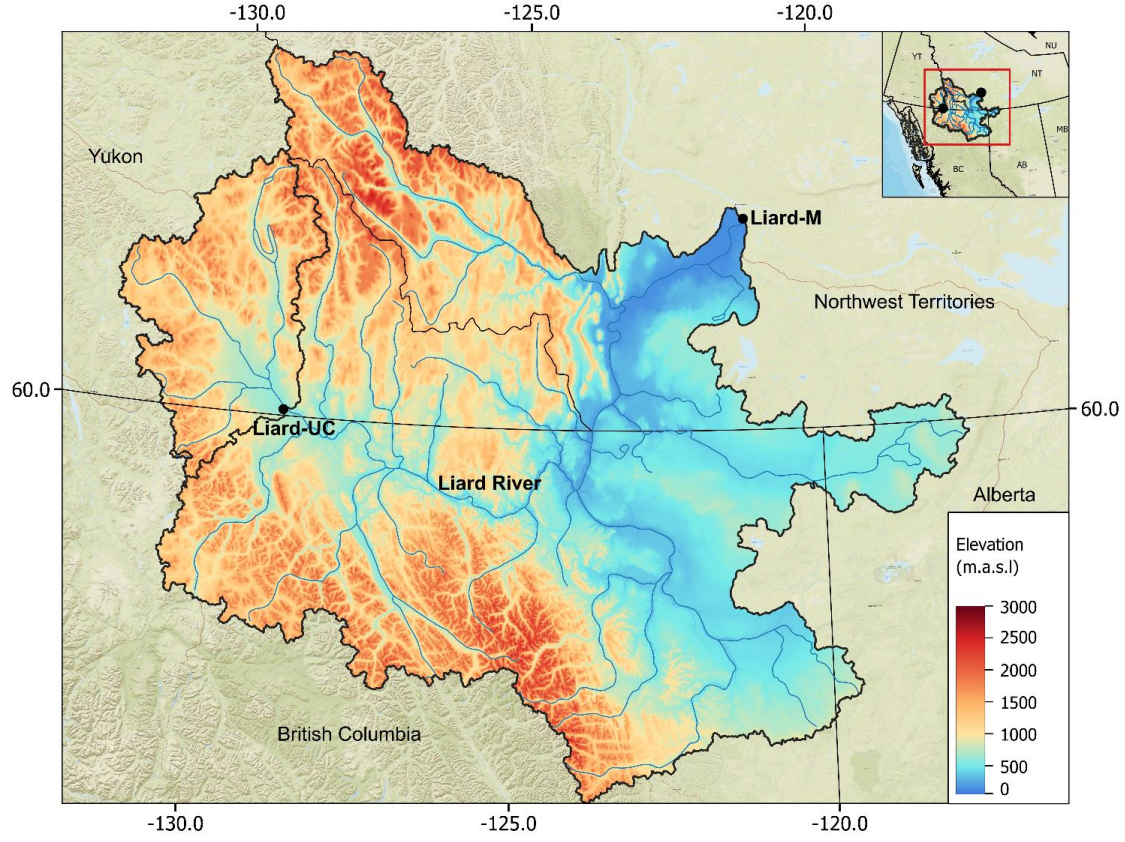

Figure 1. Location map of the Liard River basin. Also shown are the outlets of the Liard-M and Liard-UC basins for which analyses were performed.

3. Models, Data and Analyses

3.1 Hydrologic models

We employed the Variable Infiltration Capacity (VIC) hydrologic model version 5.0.0 (Liang et al., 1994, 1996; Hamman et al., 2018), set up at a 1/16° spatial resolution for the LRB (Shrestha et al., 2019, 2022), as a benchmark WHM. VIC is a process-based, semi-distributed hydrologic model that accounts for sub-grid variability in snow and vegetation. Since its initial development in the 1990s, the model has undergone several updates and refinements, including key cold-regions processes of energy balance over snow and frozen ground (Cherkauer and Lettenmaier, 1999, 2003; Andreadis et al., 2009). VIC has been used extensively for assessing the hydrologic impacts of climate change across cold-region river basins (Schnorbus et al., 2014; Chegwidden et al., 2019; Shrestha et al., 2019; Eum et al., 2016).

We compared the Community Water Model (CWatM) version 1.081, a large-scale semi-distributed GHM developed for regional to global scale hydrologic applications (Burek et al., 2020), with the VIC model. CWatM was developed with the philosophy of as complex as necessary but not more (Burek et al., 2020), and different hydrologic processes, including cold-region processes of snow accumulation and melt, are represented. Similar to VIC, it accounts for sub-grid variability in snow and land cover. CWatM has been used for streamflow simulation in several global-scale assessments (Burek et al., 2020; Greve et al., 2020;

https://doi.org/10.5194/egusphere-2024-3170
Preprint. Discussion started: 22 November 2024

Heinicke et al., 2024), and as part of a multi-GHM ensemble for future projections of floods, water shortage and drought (Boulange et al., 2021; Pokhrel et al., 2021; Satoh et al., 2022). However, to our knowledge, applications specifically focused on cold-regions are not available. For this study, we used the 5-arc-minute (or 1/12°) resolution CWatM configuration, including the static geospatial data made available by the model developers (ftp://rcwatm:Water1090@ftp.iiasa.ac.at/).

As summarized in Table 1, the two model setups have a major difference in the number of subbasins, with VIC subdivided into 28 subbasins and CWatM subdivided into two subbasins. While it is technically feasible to subdivide the CWatM setup to match the VIC subbasin structure, setting up and running it over 28 subbasins will be cumbersome, because like most GHMs, CWatM is designed for large-scale applications and not for running over nested subbasins with multiple parameter sets. Furthermore, we wanted to apply these models as they are designed to be used: a GHM at large basin scale, and a WHM over multiple subbasins. Nevertheless, we set up CWatM for the Liard River at Upper Crossing (Liard-UC) subbasin to compare with the VIC model setup (Liard-UC is further subdivided into three subbasins in VIC) for a relatively small subbasin (drainage area = 32,600 km^2). Besides the number of subbasins, the two model setups also differ in terms of spatial resolution and base geospatial datasets (soil, land cover and digital elevation model) (Table 1).

The representations of hydrologic processes in VIC and CWatM are mostly similar, except for subsurface flow, snow and frozen ground (Table 2). Specifically, the three-component runoff generation processes in CWatM, consisting of direct runoff, interflow and baseflow, differ from the two-component formulation in VIC, consisting of surface runoff and subsurface flow (baseflow). The presence of groundwater storage in CWatM can be expected to lead to delayed baseflow response, compared to VIC without groundwater storage and baseflow response represented by a nonlinear function. Additionally, differences in snowmelt methods, consisting of full energy balance in VIC and radiation-restricted approach in CWatM, can potentially lead to differences in snowmelt and runoff outputs. Finally, the coupled soil thermal and moisture flux process representation in VIC, which is used to control soil water movement through frozen soil, contrasts with the simple frost index method used to restrict soil water movement in CWatM. These differences can be expected to influence runoff generation pathways and consequently streamflow simulation. Additionally, the differences in calibration parameters (Table 1) can be expected to influence streamflow simulation.

Table 1. Model resolution, geospatial and meteorological datasets and model calibration for the VIC and CWatM model setups in this study

	VIC	CWatM
Spatial resolution	1/16°, sub-grids for vegetation and elevation bands snow.	1/12°, sub-grids for land cover and elevation bands for snow.
Digital elevation model	7.5 arc-second Global Multiresolution Terrain Elevation Data 2010 (Danielson and Gesch, 2011)	3 arc-second from the National Aeronautics and Space Administration Shuttle Radar Topographic Mission (Hole-filled seamless SRTM data V4 583, 2024)
Land cover	250-m land cover dataset from North American land change monitoring system (Latifovic et al., 2012)	1 arc-second forest land cover (Hansen et al., 2013), 5 arc-minute land use dataset with crop groups from Hyde 3.2 database (Klein Goldewijk et al., 2017)
Soil	1/12° soil classification and	30 arc-second from Harmonized World Soil Database 1.2 (FAO, 2012)

https://doi.org/10.5194/egusphere-2024-3170
Preprint. Discussion started: 22 November 2024

	parameterization dataset based on the Soils Program in the Global Soil Data Products CD-ROM (Global Soil Data Task, 2014)	
Temporal resolution/ Meteorological inputs	3 hourly: average air temperature, total precipitation, wind speed, atmospheric pressure, incoming shortwave radiation, incoming longwave radiation, vapor pressure. Disaggregated and generated from daily from maximum and minimum air temperature, total precipitation, wind speed (PNWNAmet datasets (Werner et al., 2019) and downscaled GCMs) using MTCLIM in-built in the VIC model (Thornton et al., 2000)	Daily: average, maximum and minimum air temperature, total precipitation, wind speed, atmospheric pressure, relative humidity, incoming shortwave radiation, incoming longwave radiation. Generated from daily maximum and minimum air temperature, total precipitation, wind speed (PNWNAmet datasets (Werner et al., 2019) and downscaled GCMs) using MTCLIM/MetSim (Thornton et al., 2000; Bennett et al., 2020)
Model calibration	Model calibrated at the outlets of 28 subbasins by comparing with the discharge data from the Water Survey of Canada hydrometric stations (wateroffice.ec.gc.ca). Calibration using the nondominated sorting genetic algorithm (NSGA-II) (Deb et al., 2002). Best performing model selected from the trade-off of three objective functions: (i) Nash–Sutcliffe coefficient of efficiency (NSE), (ii) NSE of log-transformed discharge (LNSE), and (iii) volume bias (VB) using fuzzy preference selection method (Shrestha and Rode, 2008). Calibration period: 1984-1993; Validation period: 1994-2003.	Model calibrated at the outlet of 2 subbasins only (headwaters: Liard-UC, outlet: Liard-M) by comparing with observed discharge from the Water Survey of Canada hydrometric stations (wateroffice.ec.gc.ca). Calibration using the single objective version of the NSGA-II (Deb et al., 2002) as implemented in the Python DEAP package (Fortin et al., 2012) with KGE criteria (Gupta et al., 2009). Calibration period: 1984-1993; Validation period: 1994-2003.
Calibration parameters	Six parameters: variable infiltration curve parameter; fraction of maximum soil moisture for nonlinear baseflow; maximum velocity of baseflow; fraction of maximum velocity for nonlinear baseflow; and saturated hydraulic conductivity with soil moisture.	Ten parameters: snowmelt coefficient; crop factor for ET; soil depth factor; preferential flow constant; infiltration capacity; interflow factor; groundwater recession coefficient; runoff concentration; Mannings n; reservoir normal storage limit.

140

https://doi.org/10.5194/egusphere-2024-3170
Preprint. Discussion started: 22 November 2024

Table 2. Summary of key physical process representation in the VIC and CWatM models as used in this study

	VIC	CWatM
Potential evapotranspiration	Penman-Monteith equation with canopy resistance set to zero (Shuttleworth, 1993)	FAO Penman-Monteith with hypothetical reference vegetation (Allen et al., 1998)
Snow accumulation and melt	2-layer energy balance snow model (Andreadis et al., 2009)	Radiation-restricted degree-day factor (Erlandsen et al., 2021) – introduced in CWatM version 1.081 – modified for this study to account for snow albedo decay as in the VIC model (https://github.com/aranhax/CWatM).
Infiltration	Xinanjiang infiltration capacity method (Zhao and Liu, 1995)	Xinanjiang infiltration capacity method (Zhao and Liu, 1995)
Soil water movement	Unsaturated flow through 3-layer soil column using one-dimensional Richard's equation.	Unsaturated flow through 3-layer soil column using one-dimensional Richard's equation.
Runoff components, groundwater storage and baseflow	Two component runoff: surface runoff and baseflow. Groundwater storage not available, ARNO baseflow recession curve for drainage from bottom soil layer, with parameters controlling non-linear baseflow (Franchini and Pacciani, 1991).	Three component runoff: direct runoff, interflow (that contributes to both surface runoff and groundwater) and baseflow. Groundwater storage using linear reservoir approach, and baseflow a function of groundwater storage and recession coefficient (Burek et al., 2020).
Frozen ground	Soil thermal and moisture fluxes are coupled processes, with soil water movement under frozen soil condition dependent on ice content. Ground heat flux through the soil temperature profile using the finite difference method and no flux boundary (Cherkauer and Lettenmaier, 1999, 2003).	No frozen soil formulation, empirical frost index method (Molnau and Bissell, 1983) to consider frozen soil state and restrict soil water movement through top two layers.
River routing	Linearized version of the Saint-Venant equations, with impulse response functions (i.e. unit-hydrographs) to represent distribution of flow at the outlet point (Lohmann et al., 1998).	Kinematic wave approximation of the St. Venant equation (Chow, 2010) with coefficients calculated using Manning's equation.

3.2 Climate data and downscaling

We used daily temperature, precipitation and wind speed from the Pacific North Western North America gridded meteorological data PNWNAmet (Werner et al., 2019) as inputs for the calibration of both the VIC and CWatM models, and as the target dataset for statistical downscaling (Table 1). PNWNAmet is a spatially contiguous and temporally consistent dataset spanning the years 1945-2012, which has been found to outperform other gridded observational data products available for the region in terms of climate means, extremes and variability, as well as streamflow trends and runoff ratios when used to drive the VIC model (Werner et al., 2019). The PNWNAmet dataset has a spatial resolution of 1/16°, matching the resolution of the VIC model used in this study.

https://doi.org/10.5194/egusphere-2024-3170
Preprint. Discussion started: 22 November 2024

We used an ensemble of eight CMIP6 GCMs (summarized in ESM Table S1) based on the GCM selection by Mahony et al. (2022) for the Intergovernmental Panel on Climate Change (IPCC) reference Northwestern North America region. The GCM selection methodology uses ten different criteria, and the selected eight-model subset represents the very likely range of Earth's equilibrium sensitivity according to IPCC's recent assessment (Arias et al., 2021). For each GCM, we considered historical period (1950-2014) and two shared socioeconomic pathways (SSP), consisting of high (SSP5-8.5) and moderate (SSP2-4.5) scenarios over the years 2015-2100. Thus, uncertainties due to GCM structure and greenhouse gas concentration and anthropogenic forcings pathways – which are the most important sources of uncertainties in projecting hydrologic impacts of climate change (Hattermann et al., 2018; Chegwidden et al., 2019) – are considered in this study.

We employed a state-of-the-art N-dimensional probability density function transform, multivariate bias correction method (MBCn) (Cannon, 2018a, b) to spatially disaggregate and bias-correct coarse-resolution GCM outputs, consisting of daily precipitation, maximum and minimum temperature and wind speed, to the 1/16° resolution of the PNWNAmet dataset. This method preserves multivariate dependence of the target observational data, which is an important consideration for multivariate climate extremes (Zscheischler et al., 2018) and cold-regions hydrologic processes, such as precipitation and temperature interactions on snow accumulation and melt processes (Meyer et al., 2019; Warden et al., 2024). MBCn builds on an image processing technique (Pitié et al., 2007) that operates by iteratively (i) applying a random orthogonal rotation to both climate model and observational target datasets, (ii) correcting the marginal distributions via quantile mapping, and (iii) rotating datasets back to the original axes and checking convergence. The iterative steps ensure the transfer of the climate model's marginal distributions and empirical copula in the historical calibration period to those of observations. For the future period, projected changes in the corrected quantiles are also constrained to match those of the raw climate model. We used the 63-year 1950–2012 period for calibration of MBCn, with bias corrections applied over three 21-year sliding window blocks to match the length of the calibration period. For further details on the MBCn, readers are referred to Cannon (2018a).

Both PNWNAmet and downscaled GCMs required pre-processing before they could be used as inputs to the VIC and CWatM models. For VIC, we employed the built-in Mountain Microclimate Simulation Model (MTCLIM) (Thornton and Running, 1999) to disaggregate and generate 3-hourly meteorological inputs of precipitation, maximum and minimum air temperature, wind speed, longwave radiation, shortwave radiation, atmospheric pressure and vapor pressure for running it in an energy balance mode. For CWatM, we first regridded the daily maximum and minimum air temperature, total precipitation and wind speed from both PNWNAmet and downscaled GCMs to the CWatM model resolution of 1/12° by using bilinear interpolation. We then used the MTCLIM method, available in the Python Meteorology Simulator package (Bennett et al., 2020), to generate additional daily inputs required for CWatM, which include longwave radiation, shortwave radiation, atmospheric pressure and relative humidity. After calibrating VIC and CWatM with the pre-processed PNWNAmet dataset as inputs, we forced the two models with pre-processed CMIP6 GCMs over the transient period 1950-2100, by combining historical and SSP scenarios. Hence, this study updates the CMIP5 GCM driven VIC model simulations from previous studies (Shrestha et al., 2019, 2022) with CMIP6 GCMs.

3.3 Evaluation methods and metrics

We evaluated the performance of calibrated VIC and CWatM models by comparing simulated results against observations using four goodness-of-fit (GOF) metrics: (i) Nash Sutcliffe coefficient of efficiency (NSE) (Nash and Sutcliffe, 1970); (ii) NSE of log-transformed discharge (LNSE); (iii) Kling-Gupta efficiency (KGE) (Gupta et al., 2009); and (iv) volume bias (VB). NSE, LNSE and KGE values closer to one represent a better model fit, whereas volume bias close to zero indicates a better model fit.

https://doi.org/10.5194/egusphere-2024-3170
Preprint. Discussion started: 22 November 2024

Following the IPCC Working Group I sixth assessment (AR6) (Arias et al., 2021), we analyzed model results at 1.5, 2.0, 3.0 and 4.0 °C global warming levels (GWLs) above the preindustrial period of 1850–1900. The period when each GWL is reached for individual GCMs depends on its climate sensitivity, as different GCMs respond very differently to the same combination of radiative forcings (Smith et al., 2020). Since we used bias-corrected GCMs, we calculated GWLs for individual GCMs relative to the recent period of 1995-2014 by assuming 0.85 °C warming between 1850-1900 and 1995-2014, which is the amount of observed temperature increase reported in IPCC AR6 (Gulev et al., 2021). As summarized in ESM Table S1, not all GCMs reach the 3.0 and 4.0 °C GWLs by the end of their simulations in the year 2100. We analyzed projected responses at each GWL by combining all available ensemble members of SSP5-8.5 and SSP2-4.5 scenarios, which consist of 16 ensemble members for 1.5 and 2.0 °C GWLs, and 12 and 6 ensemble members for 3.0 and 4.0 °C GWL, respectively. We considered the 30-year climatological period of 1971-2000 as the reference period – which corresponds to observed warming of approximately 0.5 °C since the preindustrial period (Forster et al., 2023) – to compare future projections at the four GWLs. The projected responses were analyzed for a set of responses (annual water balance, monthly flow and snow water equivalent, annual maximum streamflow and timing, and flood frequencies), by comparing the range, magnitude, and direction of changes relative to the reference period, and the percentage agreement of the ensemble members with the direction of median change.

We analyzed extreme value statistics of annual maximum flows for the 1971-2000 reference period and four GWLs by combining all annual maximum flow values from all models in the ensemble. The combined sample sizes for 1971-2000 and 1.5, 2.0, 3.0 and 4.0 °C GWLs are 240 (30 years x 8 members), 256 (20 x 16), 256 (20 x 16), 240 (20 x 12) and 120 (20 x 6), respectively. The use of combined annual maximum flow values from all GCM and SSP ensemble members – following a similar approach by Curry et al. (2019) – provides adequate samples for analyzing large return periods (e.g., 100 and 200 years), with the assumption that the reference period and each GWLs can be considered roughly stationary. We fitted a generalized extreme value (GEV) distribution to the samples by using the maximum likelihood parameter estimation (Hosking and Wallis, 1993), as implemented in the R 'extRemes' package (Gilleland, 2024).

4 Results and discussion

4.1 Hydrologic model calibration/validation

We present simulated streamflow results for the Liard River at Mouth (Liard-M) station as an aggregate response for the entire LRB, and for the Liard River at Upper Crossing (Liard-UC) station as a subbasin response (Fig. 2). The simulated results, in general, indicate a good ability of both VIC and CWatM to reproduce the dynamics of streamflow hydrograph, characterized by high snowmelt-driven flow during spring and summer and low flow in winter. However, both models have difficulty in matching the magnitude of the peak flow at both stations. Additionally, CWatM tends to produce earlier peak flows than observations and VIC simulations, especially for the Liard-M station (Fig. 2a). CWatM also underpredicts winter low flows at Liard-M, while VIC provides a better match. For the Liard-UC station, CWatM results match with observations and VIC results better, both for low and high flows.

The comparison of the statistical GOF metrics of NSE, LNSE, KGE and VE reveals generally better performance of VIC compared to CWatM (Table 3). Additionally, while VIC results are similar for the Liard-UC and Liard-M stations, CWatM performed better for Liard-UC than Liard-M. Several factors likely contribute to these differences. Firstly, the subdivision of the LRB into 28 subbasins allows VIC to parameterize and calibrate to subbasin-specific conditions (6 parameters x 28 subbasins in total), and the use of calibrated upstream flows as inflows help to better match the flows at the outlets of Liard-UC and Liard-M.

https://doi.org/10.5194/egusphere-2024-3170
Preprint. Discussion started: 22 November 2024

In contrast, since CWatM was calibrated by lumping the large LRB into only two sets of parameters (10 parameters x 2 subbasins), it is not able to capture the subbasin-level heterogeneity. Additionally, the aforementioned differences in model structure, especially those related to frozen ground and groundwater, affect the runoff generation processes and subsequently model performance. Particularly, the frost index method in CWatM, which prevents infiltration through the top two soil layers under frozen soil condition, likely leads to a higher proportion of surface runoff and contributes to earlier peak flows in CWatM compared to VIC, which allows infiltration through frozen soil using the coupled soil thermal and moisture flux representation (Cherkauer and Lettenmaier, 2003). Besides these model related differences, both model results are also affected by uncertainties associated with input and calibration data. Specifically, the representativeness of the precipitation and temperature in the PNWMAmet dataset due to sparse station density at high-latitude region (Werner et al., 2019), and limitations in observed discharge estimation during ice-covered and ice breakup events (Hamilton and Moore, 2012) can be major sources of uncertainty.

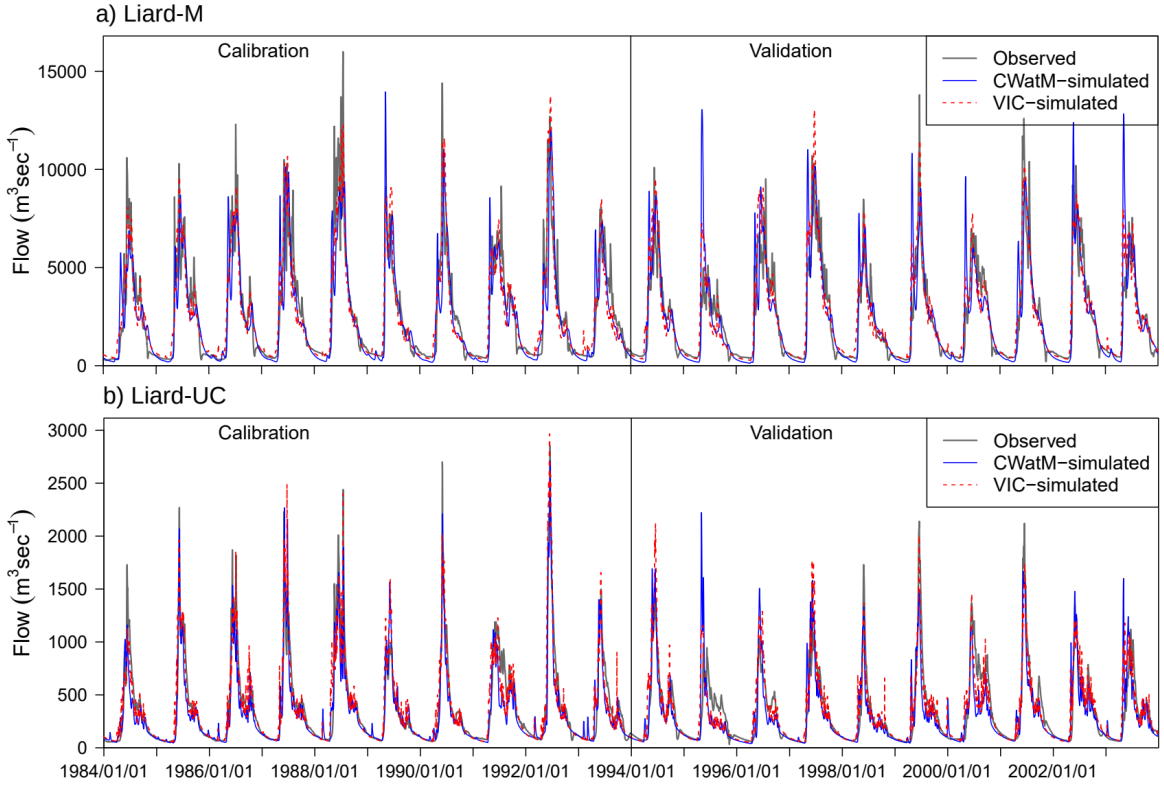

Figure 2. Observed vs. simulated discharge from CWatM and VIC models for calibration (1984-1994) and validation (1994-2004) periods for a) Liard-M station and b) Liard-UC station.

https://doi.org/10.5194/egusphere-2024-3170
Preprint. Discussion started: 22 November 2024

Table 3. Comparison of the goodness-of-fit (GOF) metrics for VIC and CWatM results. Summarized metrics include Nash-Sutcliffe coefficient of efficiency (NSE), NSE of log flows, Kling-Gupta coefficient (KGE) and % volume bias (VB) for calibration (validation) 1984-1993 (1994-2003).

Basin/ Subbasin	VIC				CWatM			
	NSE	LNSE	KGE	VB	NSE	LNSE	KGE	VB
Liard-M	0.86 (0.83)	0.87 (0.88)	0.92 (0.90)	-1.6 (4.3)	0.72 (0.65)	0.82 (0.79)	0.83 (0.82)	-6.4 (2.0)
Liard-UC	0.86 (0.79)	0.88 (0.83)	0.92 (0.89)	-2.0 (-0.9)	0.86 (0.68)	0.89 (0.80)	0.82 (0.81)	-6.4 (-4.2)

Further, the comparison of VIC and CWatM simulated snow water equivalent (SWE) with observations at three snow pillow sites with highest number of observations generally shows a good replication of the seasonal dynamics by both models (Supplement Fig. S1). Specifically, the seasonal SWE accumulation and ablation, as well as maximum SWE values are reasonably well replicated by both models. The good model performance is also indicated by GOF values (Table S2). The SWE simulations from both models are also affected by uncertainties related to model structure and meteorological inputs, as discussed earlier. Additional sources of uncertainty include the mismatches between the observation station location and elevation with the model grid and elevation band, respectively, and measurement errors (e.g., SWE calculation from snow depth). Nevertheless, given the reasonable replication of the magnitude and dynamics of observed SWE and streamflow, as well as VIC simulated values, the calibrated CWatM model can be considered suitable for projecting future hydrologic responses.

4.2 Temperature and precipitation changes

Before evaluating projected future hydrologic responses from VIC and CWatM, we analyzed the MBCn downscaled temperature and precipitation from the GCM ensemble. As expected, the seasonal and annual temperature and precipitation over the LRB show progressive increases with the GWLs (Fig. 3). Furthermore, consistent with the projected higher warming over northern latitudes (Flato et al., 2019), the basin-scale seasonal and annual temperatures increases are higher than global temperature increases, with median increases of +1.8, +2.6, +4.1, and +5.6 °C relative to the 1971-2000 period at +1.5 (or +1.0 global warming from 1971-2000), +2.0 (+1.5), +3.0 (+2.5) and +4.0 (+3.5) °C GWLs, respectively. Seasonally, higher temperature increases are projected for the colder months (OND and JFM) than warmer months (AMJ and JAS).

The projected annual precipitation in the LRB mostly shows progressive increases with GWLs, with median basin-scale annual increases of 6.5, 8.8, 16.9, and 24.3% relative to the 1970-2000 reference period at 1.5, 2.0, 3.0 and 4.0 °C GWLs, respectively. Seasonally, projected precipitation for most GCMs shows increases, with a larger variability of change for AMJ and smaller variability for OND. The median seasonal precipitation increases are largest in OND, except for the larger increases in AMJ at 4.0 °C GWL. Overall, the enhanced temperature and precipitation increases for CMIP6 GCMs over the LRB are similar to CMIP5 GCMs assessed in our previous study (Shrestha et al., 2019).

https://doi.org/10.5194/egusphere-2024-3170
Preprint. Discussion started: 22 November 2024

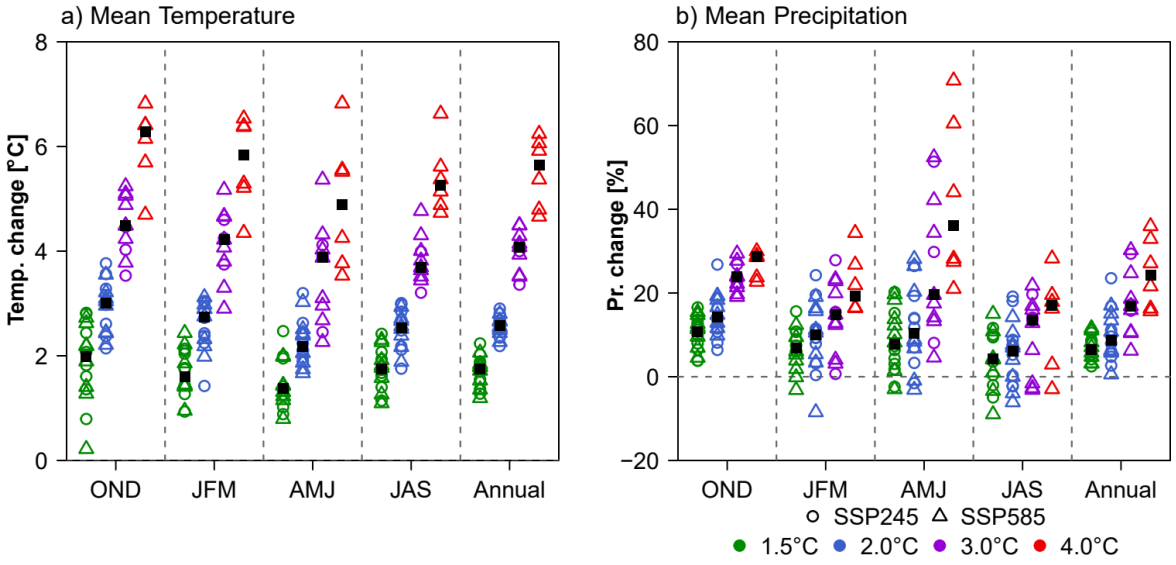

Figure 3. Mean annual and seasonal temperature and precipitation changes at 1.5 to 4.0 °C GWL relative to 1971-2000 reference period. The projected changes for SSP2-45 and SSP5-85 scenarios are shown together.

4.3 Annual water balance change

We first compared the VIC and CWatM model simulations of annual water balance variables, consisting of precipitation, evapotranspiration (ET) and runoff, averaged over the entire LRB (Fig. 4). Additionally, we assessed maximum SWE (SWEmax), as it is related to all water balance variables. The results from the two models depict very similar changes, characterized by progressive increases in annual ET and runoff in response to increasing precipitation and temperature. SWEmax changes are minimal at the four GWLs for both models, suggesting that the projected winter precipitation increases offset the temperature-driven snowpack declines. The ranges of median percentage changes are generally similar, and models typically agree on the direction of median change, except for the small changes in SWEmax.

The results are consistent when comparing the distribution of precipitation into ET and runoff. Specifically, for both models, the median ET/precipitation ratios range between 0.45 and 0.48, while the runoff/precipitation ratios range between 0.52 and 0.55, with generally decreasing ET/precipitation ratios and increasing runoff/precipitation ratios at higher GWLs. Furthermore, the median SWEmax/October-March precipitation ratios, with a ratio > 0.5 used to characterize the hydrologic regime of a basin as snow-dominated (Elsner et al., 2010), decline successively from 0.84 to 0.65 with higher GWLs for both models. Overall, the projected annual water balance changes from CWatM are consistent those from VIC.

https://doi.org/10.5194/egusphere-2024-3170
Preprint. Discussion started: 22 November 2024

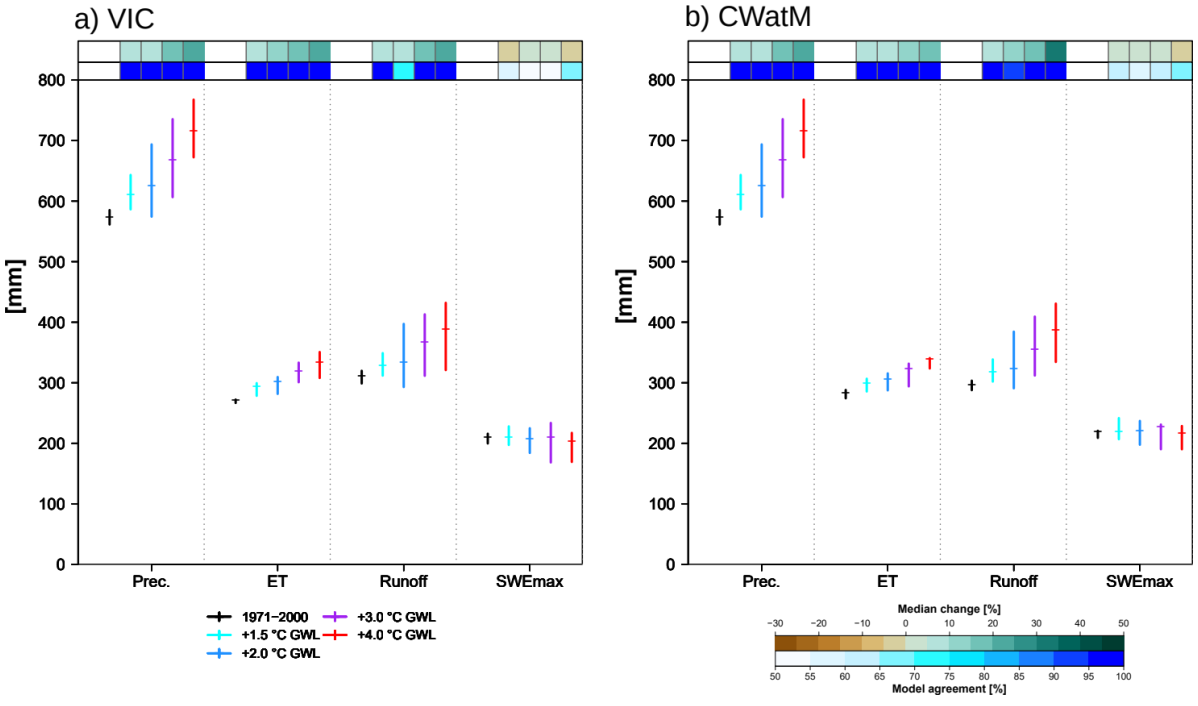

Figure 4. Historical (1971-2000) and projected annual water balance variables (mm) at 1.5 to 4.0 °C global warming levels (GWLs) obtained from the GCM ensemble. The results show basin-averaged values for the entire Liard River basin, consisting of precipitation used as forcings, and a) VIC and b) CWatM simulated evapotranspiration (ET), runoff and maximum snow water equivalent (SWEmax). Top panels show the median change (%) at the four GWLs relative to 1971-2000, along with the model agreement (%) of the GCM ensemble with the direction of median change.

4.4 Monthly SWE and flow changes

Changes in basin-averaged monthly SWE values from the two models at different GWLs are also generally consistent (Fig. 5). Both models show slightly higher SWE accumulation in the colder upstream Liard-UC subbasin than the entire Liard-M basin. Furthermore, monthly SWE values successively decline with higher GWLs during October and November, while the changes from December to March are relatively smaller. Monthly SWE values also decline successively with higher GWLs in April and May, with CWatM showing more rapid declines, particularly for the Liard-UC subbasin. However, the differences are marginal, and model agreement in the direction of median change is generally good between the two models for both Liard-M and Liard-UC. Additionally, both models show higher agreement in the direction of median change in the months with larger snowpack loss (October, November, May and June) and lower agreement in the months with smaller snowpack change (January to March). The generally consistent monthly SWE and SWEmax results (Figs. 4 and 5) suggest that the differences in snowmelt algorithms in two models (VIC: full energy balance; CWatM: radiation-restricted degree-day) have a minor effect on the magnitude and timing of snowmelt. However, these results may have been influenced by the necessity to calculate all energy fluxes from the same air temperature, precipitation and wind speed datasets in both models using MTCLIM.

Projected mean monthly flows (Q_{mean}) from the two models display consistent patterns, with progressive increases in cold-season (October-March) flows with higher GWLs for both Liard-M and Liard-UC stations (Fig. 6). Furthermore, both models project generally increased Q_{mean} with higher GWLs in April and May, following the declining SWE patterns for these two months (Fig.

https://doi.org/10.5194/egusphere-2024-3170
Preprint. Discussion started: 22 November 2024

5). The direction of projected Q_{mean} change in June differs between the two stations but is consistent between VIC and CWatM, with a declining pattern at higher GWLs for the upstream Liard-UC station and an increasing pattern for the downstream Liard-M station. The larger uncertainties in projected AMJ precipitation at 3.0 and 4.0 °C GWLs (Fig. 3) likely contributed to larger spreads of the projected flow responses during these months and GWLs. July and August Q_{mean} projections from the two models show some differences, with CWatM projections showing smaller declines for Liard-M and smaller decreases or increases for Liard-UC, compared to VIC, which shows larger declines for both stations. September Q_{mean} responses are consistent between the two models, with progressive increases in flows at higher GWLs. These similarities and differences in responses between the two models are also reflected by the median changes and model agreements. Specifically, both models show progressive increases in median values and high model agreement between October and May. For June to August, the median changes are less consistent, and direction of changes shows lower agreement.

These differences in VIC and CWatM projections arise from the combined effect of several factors related to process representation and parameterization. As discussed, the differences in the treatment of frozen soil processes in the two models affect infiltration and runoff pathways, with a higher proportion of surface runoff generation in CWatM than in VIC (Fig. S2) influencing early summer (June) Q_{mean}. On the other hand, the presence of groundwater storage in CWatM, which stores percolated water and releases it as baseflow using a linear reservoir approach (Burek et al., 2020), delays the baseflow response and results in a higher late summer (July and August) Q_{mean} from CWatM than from VIC, which uses a nonlinear baseflow function to release water stored in the bottom layer. Other factors that contribute to these differences include the routing method and parameterization, which influence runoff transport through the watershed and the timing and magnitude of flow delivered to the outlet, and the differences in watershed subdivision and model calibration. However, despite the inferior calibration performance for the downstream Liard-M station (Table 3), CWatM projection results for this station are not substantially different from VIC results. This suggests that the uncertainties in projected responses due to lumped parameters and calibration may be relatively small.

https://doi.org/10.5194/egusphere-2024-3170
Preprint. Discussion started: 22 November 2024

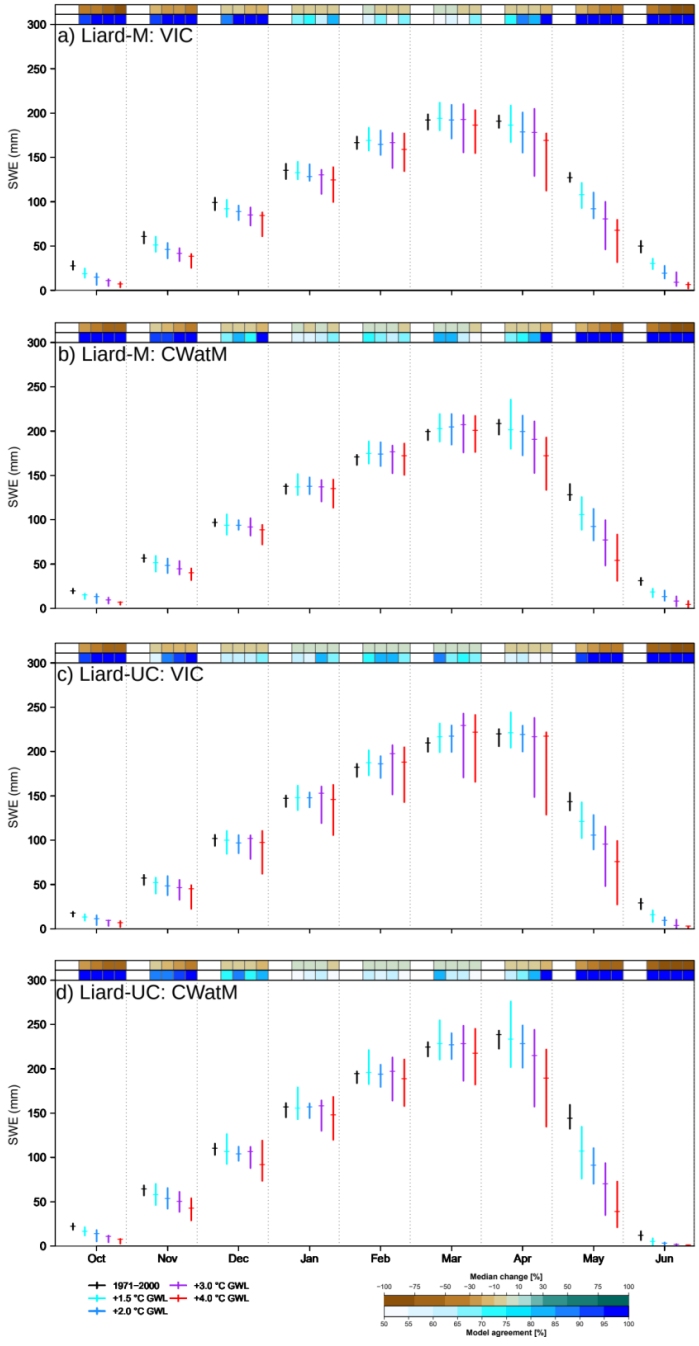

330 **Figure 5.** Historical (1971-2000) and projected monthly SWE (mm) at 1.5 to 4.0 °C global warming levels (GWLs) obtained from the GCM ensemble. All SWE results are simulated basin-averaged values from model simulations, consisting of a) VIC for Liard-M station, b) CWatM for Liard-M station, c) VIC for Liard-UC station, and d) CWatM for Liard-UC station. Top panels show median change (%) at four GWLs relative to 1971-2000, along with model agreement (%) of the GCM ensemble with the direction of median change.

https://doi.org/10.5194/egusphere-2024-3170
Preprint. Discussion started: 22 November 2024

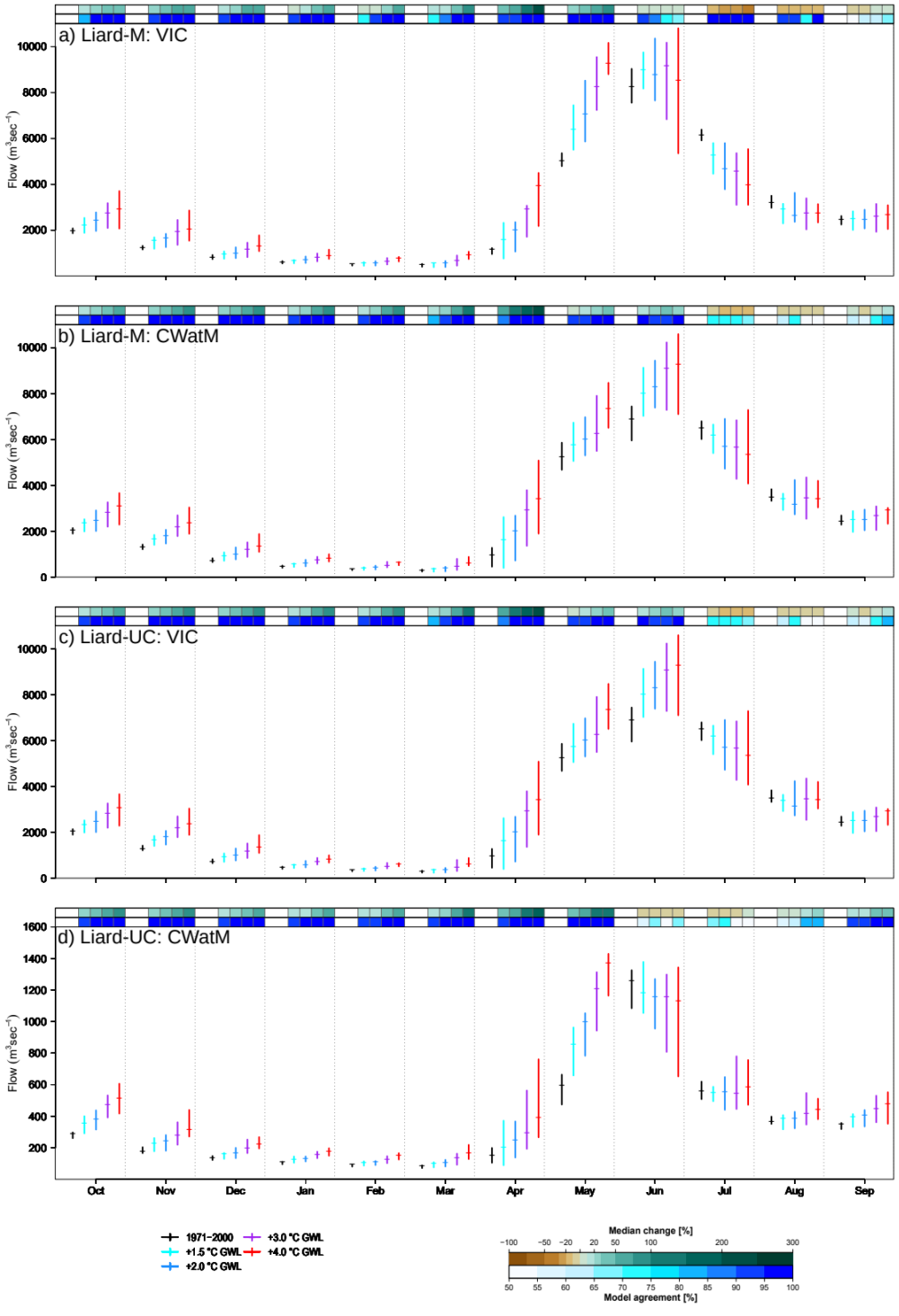

335

Figure 6. Same as Figure 4, but for monthly flows.

https://doi.org/10.5194/egusphere-2024-3170
Preprint. Discussion started: 22 November 2024

4.5 Maximum flow and timing

Projected changes in maximum flows (Q_{max}) and their timing are generally consistent between the two models in terms of the direction of change and are seen to be dependent on GWLs, with progressively higher Q_{max} values and earlier Q_{max} timing with higher GWLs for both Liard-M and Liard-UC (Fig. 7). However, while the median Q_{max} values and timing are similar between the two models for Liard-UC, Liard-M Q_{max} values are generally smaller and Q_{max} timing occurs earlier for CWatM, compared to corresponding projections from VIC.

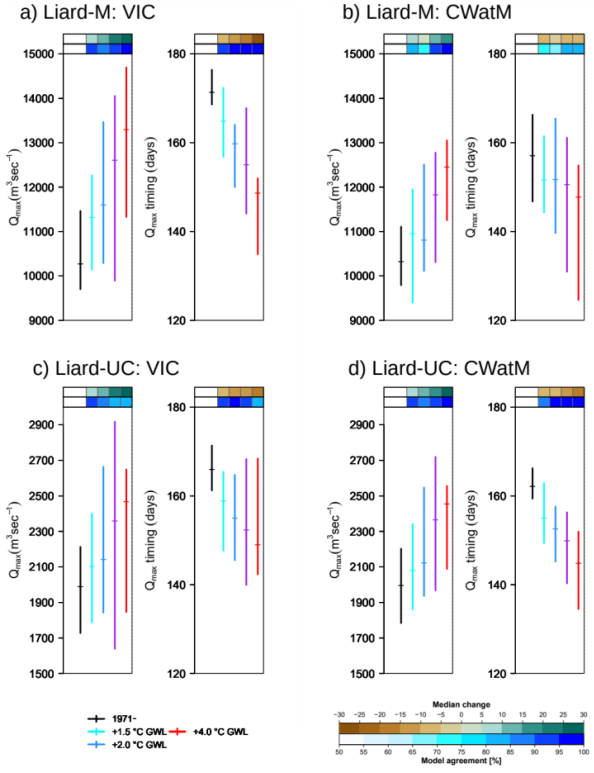

Figure 7. Same as Figure 4, but for annual maximum flows and their timing. Top panels show median change (% or days) at four GWLs relative to 1971-2000, along with the model agreement (%) of the GCM ensemble with the direction of median change.

The 2 to 200-year flood frequency curves show progressively higher flow values at a given return period at 2.0 and 4.0 °C GWLs compared to the 1971-2000 reference period for both models and stations (Fig. 8). An alternative interpretation of these nonstationary changes is that the return periods associated with specific magnitudes of flow decrease with higher GWLs. Increasing spreads of the 95% confidence intervals from 2 to 200-year return periods can also be seen from both models and stations. Interestingly, the flood frequency curve for Liard-M at 3.0 °C GWL (Fig. S3) covers a higher range than at 4.0 °C for both models, especially at higher return periods (> 40-year for VIC and > 80-year for CWatM). Although such patterns are not present for the Liard-UC station, the results for 4.0 °C GWL are affected by a smaller sample size (6*20 values) compared to 3.0 °C (12*20 values); given that 6 and 12 out of 16 ensemble members reach 3.0 and 4.0 °C GWLs, respectively.

https://doi.org/10.5194/egusphere-2024-3170
Preprint. Discussion started: 22 November 2024

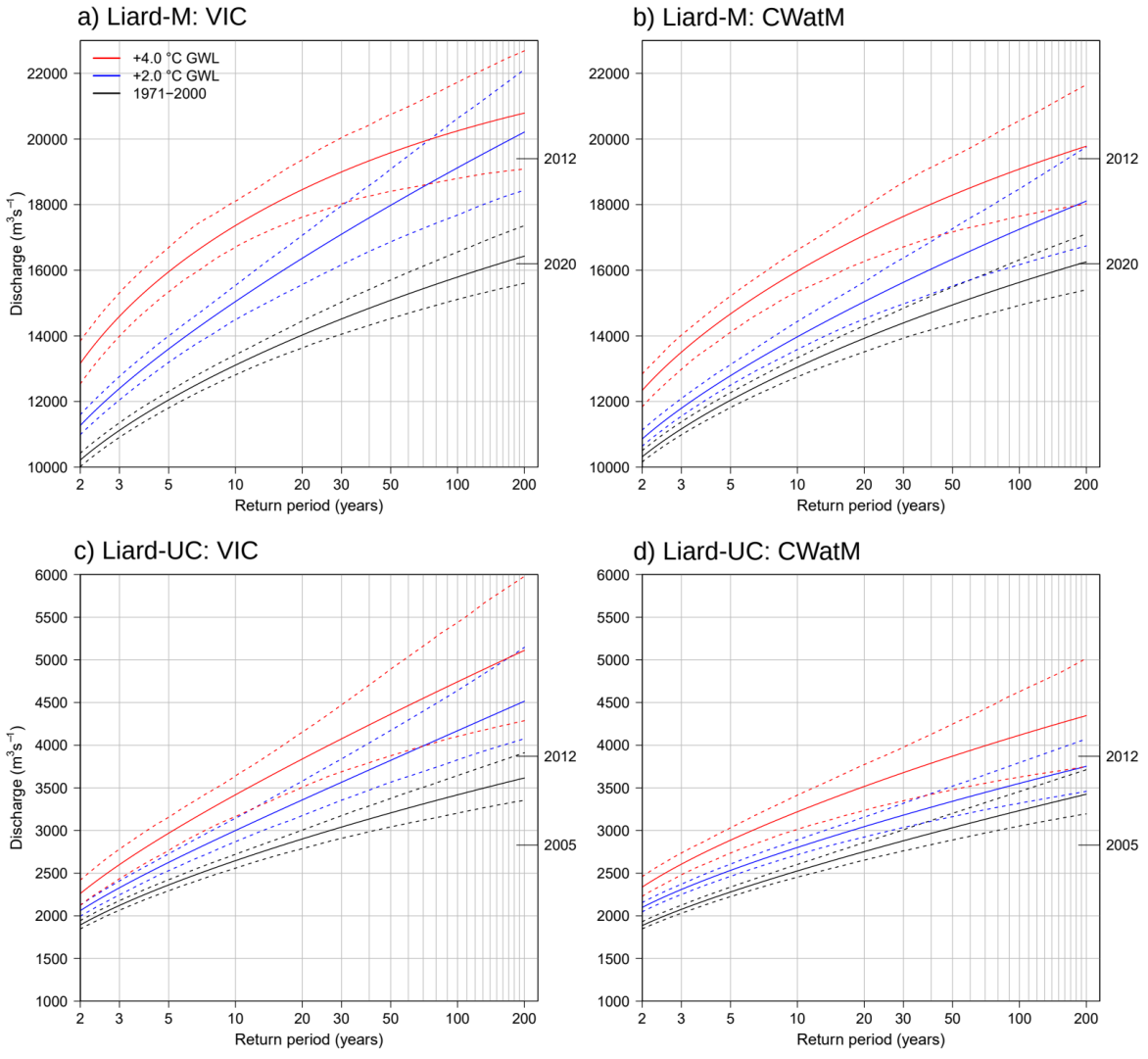

355

Figure 8. Flood frequency plots of annual maximum flows obtained from the model simulations driven by the GCM ensembles: a) VIC for Liard-M station, b) CWatM for Liard-M station, c) VIC for Liard-UC station, and d) CWatM for Liard-UC station. The results are shown for the historical period (1971-2000) and 2.0 and 4.0 °C GWLs. Dashed lines show the 95% confidence intervals. The years on the right axes of each plot indicate the two highest recorded historical flood events.

360 Additionally, while the flood frequency curves are similar for the 1971-2000 reference period for the two models, the curves tend to diverge at higher GWLs and return periods, and the magnitudes of extreme flows at a specific return period are considerably lower for CWatM than VIC (Fig. 8). For Liard-UC, it is notable that extreme flow values from the flood frequency curves are substantially lower for CWatM than corresponding values for VIC, although the median values from the two models are close to each other (Fig. 7). The divergence in responses arises from the differences in distribution of the entire ensemble, with higher
365 upper limit of VIC projections contributing to higher values in the flood frequency curves for both stations. As such, while the largest recorded 2012 flood events are within the range of the flood frequency curve at 1.5 °C GWL for VIC for both stations, they are only covered at 3.0 or 4.0 °C GWL for CWatM (Figs. 8 and S3).

https://doi.org/10.5194/egusphere-2024-3170
Preprint. Discussion started: 22 November 2024

As in the case of Q_{mean}, the magnitudes and timing of Q_{max} are affected by structural differences in the two models, particularly runoff pathways. Specifically, the earlier Q_{max} timing in CWatM than VIC can be linked to the higher fraction of quicker-flowing surface runoff in the former (Fig. S2), resulting from the frost index method that prevents soil water movement through the frozen soil. The higher Q_{max} from VIC compared to CWatM can be linked to the lack of groundwater storage in the former, which causes baseflow to increase rapidly using a nonlinear function when soil moisture exceeds a certain threshold and gets added to the total runoff (Fig. S2). Hence, the lack of groundwater storage in VIC likely causes an overestimation of annual maximum flows, and the lack of soil water movement through the frozen soil in CWatM likely causes an overestimation of the surface runoff contribution to the annual maximum flow and earlier annual maximum flows. However, notwithstanding these differences, key climate change signals of earlier and higher maximum flows, and nonstationary increases in the magnitudes of extreme flows are consistent between the two models.

5 Discussion and Conclusions

Our study contributes important insights on the robustness of future hydrologic projections from a GHM in comparison to a WHM. As suggested by Beven (2023), we designed a fit-for-purpose benchmarking study to compare future hydrologic projections from a state-of-the-art CWatM GHM with the widely used VIC WHM for the Liard River basin in subarctic Canada, by driving both models with a consistent set of downscaled CMIP6 climate forcings. Since the assessment focuses on a northern basin, our study provides a good case for evaluating the effects of model structure on cold-climate processes dominated by flows from snowmelt and frozen ground.

Our evaluation revealed generally consistent patterns of projected hydrologic responses from the two models in terms of annual water balance, and monthly distribution of SWE and flow. Key hydrologic change signals of increasing annual evapotranspiration and runoff with higher global warming levels are projected by both models. CWatM is also able to replicate the prominent snowpack change signals from VIC, particularly the successive declines in late spring SWE with higher GWLs. Likewise, CWatM simulates increasing winter and spring flows with higher GWLs, consistent with the VIC model simulation. The direction of maximum flow and timing changes from CWatM are generally in agreement with VIC, characterized by increasing and earlier flows with higher GWLs. However, the magnitude of annual maximum flows diverges between the two models, with CWatM generally producing lower magnitudes and earlier timing compared to corresponding VIC projections. These differences in the annual maximum flows are also reflected in the extreme value analysis, with CWatM projecting considerably smaller extreme flood events than VIC at all GWLs, especially for longer return periods.

The similarities and differences between the two model simulations lead to a subsequent question about the robustness of the projected changes. Overall, the consistency of the projected changes from the two models suggests that a calibrated GHM can provide robust projections of future hydrologic responses at annual and monthly time scales. The direction of SWE and flow changes obtained from both models are also consistent with the previous study based on CMIP5 GCMs driven VIC model simulations (Shrestha et al., 2019). An important consideration here is the process representation, particularly the representation of cold-climate processes of snow ablation and melt, and frozen soil. In this respect, CWatM produced very similar monthly and annual maximum SWE values when compared to VIC despite having a simplified radiation-restricted snowmelt module versus the full energy balance in VIC. However, these results may have been influenced by the necessity to calculate all energy fluxes based on the same air temperature, precipitation and wind speed datasets for both models using MTCLIM. Differences in the representation of frozen soil processes, however, led to differences in surface and subsurface flow pathways. Specifically, the simplified frost index approach (Molnau and Bissell, 1983) in CWatM, which prevents soil water movement through the frozen

https://doi.org/10.5194/egusphere-2024-3170
Preprint. Discussion started: 22 November 2024

soil, results in a higher fraction of surface runoff than VIC, which includes a coupled soil thermal and moisture fluxes approach, with soil water movement under frozen conditions dependent on ice content (Cherkauer and Lettenmaier, 1999, 2003). These differences in flow pathways seem to have affected late summer monthly flows and annual maximum flows, with a larger fraction of surface runoff in CWatM likely resulting in earlier annual maximum flows. Additionally, while the lack of groundwater storage in VIC likely leads to a more rapid baseflow response, and consequently an overestimation of annual maximum flow and amplified extreme values. In contrast, the groundwater storage in CWatM, albeit a simplified linear reservoir approach, likely causes a delayed baseflow response and smaller maximum flows, as well as a smaller reduction or no change in summer flows. Regarding other factors, such as the subdivision of the watershed into subbasins and model calibration, given that the projected results are not substantially different for the downstream Liard-M station despite lumped parameter sets and inferior calibration performance, their effects seem small.

Overall, CWatM GHM setup for the Liard River basin is generally able to replicate the projected hydrologic responses from VIC. The results are very consistent for directions of change and most magnitudes of change except maximum flows and summer flows. Hydrologic model structural uncertainties, specifically, the representation of frozen soil and groundwater processes, provide an explanation for the differences in the annual maximum flows and summer flows. Given such uncertainties, an important consideration is the robustness of model structure in simulating hydrologic metrics of interest for climate change impacts research (Ekström et al., 2018; Shrestha et al., 2016). In this respect, our results provide an important basis for improving not only the GHMs but also the WHMs.

Acknowledgements

We thank VIC and CWatM developers for the model codes, and Pacific Climate Impacts Consortium and CWatM developers for making available VIC and CWatM geospatial database used in this study.

Data availability

Downscaled GCM data and hydrologic simulations using VIC and CWatM will be made available upon request by contacting the corresponding author.

Author contributions

RRS and AJC conceptualized this study. RRS calibrated the CWatM and VIC models, ran CWatM simulations, conducted analyses and wrote the draft manuscript. AJC developed the MBCn downscaling method, provided code to implement the MBCn method and contributed to manuscript texts and edits. SH ran VIC simulations and provided support for analyses. MW ran the downscaling code and prepared inputs for running the models. AL tested the snow albedo feedback implementation in CWatM and contributed to manuscript edits.

Competing Interests

The authors declare that they have no competing interests.

https://doi.org/10.5194/egusphere-2024-3170
Preprint. Discussion started: 22 November 2024

References

Allen, R. G., Pereira, L. S., Raes, D., and Smith, M.: Crop evapotranspiration-Guidelines for computing crop water requirements-FAO Irrigation and drainage paper 56, Fao, Rome, 300, D05109, 1998.

Andreadis, K. M., Storck, P., and Lettenmaier, D. P.: Modeling snow accumulation and ablation processes in forested environments, Water Resources Research, 45, n/a-n/a, https://doi.org/10.1029/2008WR007042, 2009.

Arias, P. A., Bellouin, N., Coppola, E., Jones, R. G., Krinner, G., Marotzke, J., Nai, V., Palmer, M. D., Plattner, G.-K., Rogel, J., Rojas, M., Sillmann, J., Storelvmo, T., Thorne, P. W., and Trewin, B.: Technical Summary, in: Climate Change 2021 – The Physical Science Basis: Working Group I Contribution to the Sixth Assessment Report of the Intergovernmental Panel on Climate Change, Cambridge University Press, Cambridge, 35–144, https://doi.org/10.1017/9781009157896.002, 2021.

Bennett, A. R., Hamman, J. J., and Nijssen, B.: MetSim: A Python package for estimation and disaggregation of meteorological data, Journal of Open Source Software, 5, 2042, https://doi.org/10.21105/joss.02042, 2020.

Beven, K.: Benchmarking hydrological models for an uncertain future, Hydrological Processes, 37, e14882, https://doi.org/10.1002/hyp.14882, 2023.

Bierkens, M. F. P.: Global hydrology 2015: State, trends, and directions, Water Resources Research, 51, 4923–4947, https://doi.org/10.1002/2015WR017173, 2015.

Bierkens, M. F. P., Bell, V. A., Burek, P., Chaney, N., Condon, L. E., David, C. H., de Roo, A., Döll, P., Drost, N., Famiglietti, J. S., Flörke, M., Gochis, D. J., Houser, P., Hut, R., Keune, J., Kollet, S., Maxwell, R. M., Reager, J. T., Samaniego, L., Sudicky, E., Sutanudjaja, E. H., van de Giesen, N., Winsemius, H., and Wood, E. F.: Hyper-resolution global hydrological modelling: what is next?, Hydrological Processes, 29, 310–320, https://doi.org/10.1002/hyp.10391, 2015.

Bonsal, B., Shrestha, R. R., Dibike, Y., Peters, D. L., Spence, C., Mudryk, L., and Yang, D.: Western Canadian Freshwater Availability: Current and Future Vulnerabilities, Environ. Rev., 28, 528–545, https://doi.org/10.1139/er-2020-0040, 2020.

Boulange, J., Hanasaki, N., Satoh, Y., Yokohata, T., Shiogama, H., Burek, P., Thiery, W., Gerten, D., Schmied, H. M., Wada, Y., Gosling, S. N., Pokhrel, Y., and Wanders, N.: Validity of estimating flood and drought characteristics under equilibrium climates from transient simulations, Environ. Res. Lett., 16, 104028, https://doi.org/10.1088/1748-9326/ac27cc, 2021.

Burek, P., Satoh, Y., Kahil, T., Tang, T., Greve, P., Smilovic, M., Guillaumot, L., Zhao, F., and Wada, Y.: Development of the Community Water Model (CWatM v1.04) – a high-resolution hydrological model for global and regional assessment of integrated water resources management, Geoscientific Model Development, 13, 3267–3298, https://doi.org/10.5194/gmd-13-3267-2020, 2020.

Byun, K., Chiu, C.-M., and Hamlet, A. F.: Effects of 21st century climate change on seasonal flow regimes and hydrologic extremes over the Midwest and Great Lakes region of the US, Science of The Total Environment, 650, 1261–1277, https://doi.org/10.1016/j.scitotenv.2018.09.063, 2019.

Cannon, A. J.: MBC: Multivariate Bias Correction of Climate Model Outputs, 2018a.

Cannon, A. J.: Multivariate quantile mapping bias correction: an N-dimensional probability density function transform for climate model simulations of multiple variables, Clim Dyn, 50, 31–49, https://doi.org/10.1007/s00382-017-3580-6, 2018b.

Chegwidden, O. S., Nijssen, B., Rupp, D. E., Arnold, J. R., Clark, M. P., Hamman, J. J., Kao, S.-C., Mao, Y., Mizukami, N., Mote, P. W., Pan, M., Pytlak, E., and Xiao, M.: How Do Modeling Decisions Affect the Spread Among Hydrologic Climate Change Projections? Exploring a Large Ensemble of Simulations Across a Diversity of Hydroclimates, Earth's Future, 7, 623–637, https://doi.org/10.1029/2018EF001047, 2019.

Cherkauer, K. A. and Lettenmaier, D. P.: Hydrologic effects of frozen soils in the upper Mississippi River basin, Journal of Geophysical Research: Atmospheres, 104, 19599–19610, https://doi.org/10.1029/1999JD900337., 1999.

Cherkauer, K. A. and Lettenmaier, D. P.: Simulation of spatial variability in snow and frozen soil, J. Geophys. Res., 108, 8858, https://doi.org/10.1029/2003JD003575, 2003.

https://doi.org/10.5194/egusphere-2024-3170
Preprint. Discussion started: 22 November 2024

Chow, V. T.: Applied Hydrology, Tata McGraw-Hill Education, 592 pp., 2010.

Curry, C. L., Islam, S. U., Zwiers, F. W., and Déry, S. J.: Atmospheric Rivers Increase Future Flood Risk in Western Canada's Largest Pacific River, Geophysical Research Letters, 46, 1651–1661, https://doi.org/10.1029/2018GL080720, 2019.

Danielson, J. J. and Gesch, D. B.: Global multi-resolution terrain elevation data 2010 (GMTED2010), US Geological Survey, 2011.

Deb, K., Pratap, A., Agarwal, S., and Meyarivan, T.: A fast and elitist multiobjective genetic algorithm: NSGA-II, IEEE Transactions on Evolutionary Computation, 6, 182–197, https://doi.org/10.1109/4235.996017, 2002.

Döll, P., Trautmann, T., Gerten, D., Schmied, H. M., Ostberg, S., Saaed, F., and Schleussner, C.-F.: Risks for the global freshwater system at 1.5 °C and 2 °C global warming, Environ. Res. Lett., 13, 044038, https://doi.org/10.1088/1748-9326/aab792, 2018.

Döll, P., Hasan, H. M. M., Schulze, K., Gerdener, H., Börger, L., Shadkam, S., Ackermann, S., Hosseini-Moghari, S.-M., Müller Schmied, H., Güntner, A., and Kusche, J.: Leveraging multi-variable observations to reduce and quantify the output uncertainty of a global hydrological model: evaluation of three ensemble-based approaches for the Mississippi River basin, Hydrology and Earth System Sciences, 28, 2259–2295, https://doi.org/10.5194/hess-28-2259-2024, 2024.

Ekström, M., Gutmann, E. D., Wilby, R. L., Tye, M. R., and Kirono, D. G. C.: Robustness of hydroclimate metrics for climate change impact research, WIREs Water, 5, e1288, https://doi.org/10.1002/wat2.1288, 2018.

Elsner, M. M., Cuo, L., Voisin, N., Deems, J. S., Hamlet, A. F., Vano, J. A., Mickelson, K. E. B., Lee, S.-Y., and Lettenmaier, D. P.: Implications of 21st century climate change for the hydrology of Washington State, Climatic Change, 102, 225–260, https://doi.org/10.1007/s10584-010-9855-0, 2010.

Erlandsen, H. B., Beldring, S., Eisner, S., Hisdal, H., Huang, S., and Tallaksen, L. M.: Constraining the HBV model for robust water balance assessments in a cold climate, Hydrology Research, 52, 356–372, https://doi.org/10.2166/nh.2021.132, 2021.

Eum, H.-I., Dibike, Y., and Prowse, T.: Comparative evaluation of the effects of climate and land-cover changes on hydrologic responses of the Muskeg River, Alberta, Canada, Journal of Hydrology: Regional Studies, 8, 198–221, https://doi.org/10.1016/j.ejrh.2016.10.003, 2016.

Eyring, V., Bony, S., Meehl, G. A., Senior, C. A., Stevens, B., Stouffer, R. J., and Taylor, K. E.: Overview of the Coupled Model Intercomparison Project Phase 6 (CMIP6) experimental design and organization, Geoscientific Model Development, 9, 1937–1958, https://doi.org/10.5194/gmd-9-1937-2016, 2016.

FAO: Harmonized world soil database v1.2 | FAO SOILS PORTAL | Food and Agriculture Organization of the United Nations, 2012.

Flato, G., Gillett, N., Arora, V., Cannon, A. J., and Anstey, J.: Modelling future climate change, in: Canada's Changing Climate Report, edited by: Bush, E. and Lemmen, D. S., Government of Canada, Ottawa, ON, 74–111, https://doi.org/10.4095/327808, 2019.

Forster, P. M., Smith, C. J., Walsh, T., Lamb, W. F., Lamboll, R., Hauser, M., Ribes, A., Rosen, D., Gillett, N., Palmer, M. D., Rogelj, J., von Schuckmann, K., Seneviratne, S. I., Trewin, B., Zhang, X., Allen, M., Andrew, R., Birt, A., Borger, A., Boyer, T., Broersma, J. A., Cheng, L., Dentener, F., Friedlingstein, P., Gutiérrez, J. M., Gütschow, J., Hall, B., Ishii, M., Jenkins, S., Lan, X., Lee, J.-Y., Morice, C., Kadow, C., Kennedy, J., Killick, R., Minx, J. C., Naik, V., Peters, G. P., Pirani, A., Pongratz, J., Schleussner, C.-F., Szopa, S., Thorne, P., Rohde, R., Rojas Corradi, M., Schumacher, D., Vose, R., Zickfeld, K., Masson-Delmotte, V., and Zhai, P.: Indicators of Global Climate Change 2022: annual update of large-scale indicators of the state of the climate system and human influence, Earth System Science Data, 15, 2295–2327, https://doi.org/10.5194/essd-15-2295-2023, 2023.

Fortin, F.-A., De Rainville, F.-M., Gardner, M.-A. G., Parizeau, M., and Gagné, C.: DEAP: evolutionary algorithms made easy, J. Mach. Learn. Res., 13, 2171–2175, 2012.

Franchini, M. and Pacciani, M.: Comparative analysis of several conceptual rainfall-runoff models, Journal of Hydrology, 122, 161–219, https://doi.org/10.1016/0022-1694(91)90178-K, 1991.

https://doi.org/10.5194/egusphere-2024-3170
Preprint. Discussion started: 22 November 2024

Gädeke, A., Krysanova, V., Aryal, A., Chang, J., Grillakis, M., Hanasaki, N., Koutroulis, A., Pokhrel, Y., Satoh, Y., Schaphoff, S., Müller Schmied, H., Stacke, T., Tang, Q., Wada, Y., and Thonicke, K.: Performance evaluation of global hydrological models in six large Pan-Arctic watersheds, Climatic Change, https://doi.org/10.1007/s10584-020-02892-2, 2020.

Gilleland, E.: extRemes: Extreme Value Analysis, 2024.

Global Soil Data Task: Global soil data products CD-ROM contents (IGBP-DIS), Data Set, Oak Ridge Natl, Lab. Distrib. Active Arch. Cent., Oak Ridge, Tenn., doi, 10, https://dx.doi.org/10.3334/ORNLDAAC/565, 2014.

Gnann, S., Reinecke, R., Stein, L., Wada, Y., Thiery, W., Müller Schmied, H., Satoh, Y., Pokhrel, Y., Ostberg, S., Koutroulis, A., Hanasaki, N., Grillakis, M., Gosling, S. N., Burek, P., Bierkens, M. F. P., and Wagener, T.: Functional relationships reveal differences in the water cycle representation of global water models, Nat Water, 1, 1079–1090, https://doi.org/10.1038/s44221-023-00160-y, 2023.

Greve, P., Burek, P., and Wada, Y.: Using the Budyko Framework for Calibrating a Global Hydrological Model, Water Resources Research, 56, e2019WR026280, https://doi.org/10.1029/2019WR026280, 2020.

Greve, P., Burek, P., Guillaumot, L., Meijgaard, E. van, Aalbers, E., Smilovic, M. M., Sperna-Weiland, F., Kahil, T., and Wada, Y.: Low flow sensitivity to water withdrawals in Central and Southwestern Europe under 2 K global warming, Environ. Res. Lett., 18, 094020, https://doi.org/10.1088/1748-9326/acec60, 2023.

Gulev, S. K., Thorne, P. W., Ahn, J., Dentener, F. J., Domingues, C. M., Gerland, S., Gong, D., Kaufman, D. S., Nnamchi, H. C., Quaas, J., Rivera, J. A., Sathyendranath, S., Smith, S. L., Trewin, B., von Schuckmann, K., and Vose, R. S.: Changing State of the Climate System, edited by: Masson-Delmotte, V., Zhai, P., Pirani, A., Connors, S. L., Péan, C., Berger, S., Caud, N., Chen, Y., Goldfarb, L., Gomis, M. I., Huang, M., Leitzell, K., Lonnoy, E., Matthews, J. B. R., Maycock, T. K., Waterfield, T., Yelekçi, O., Yu, R., and Zhou, B., Climate Change 2021: The Physical Science Basis. Contribution of Working Group I to the Sixth Assessment Report of the Intergovernmental Panel on Climate Change, 287–422, https://doi.org/10.1017/9781009157896.004, 2021.

Gupta, H. V., Kling, H., Yilmaz, K. K., and Martinez, G. F.: Decomposition of the mean squared error and NSE performance criteria: Implications for improving hydrological modelling, J. Hydrol., 377, 80–91, https://doi.org/10.1016/j.jhydrol.2009.08.003, 2009.

Hamilton, A. S. and Moore, R. D.: Quantifying Uncertainty in Streamflow Records, Canadian Water Resources Journal / Revue canadienne des ressources hydriques, 37, 3–21, https://doi.org/10.4296/cwrj3701865, 2012.

Hamman, J. J., Nijssen, B., Bohn, T. J., Gergel, D. R., and Mao, Y.: The Variable Infiltration Capacity model version 5 (VIC-5): infrastructure improvements for new applications and reproducibility, Geoscientific Model Development, 11, 3481–3496, https://doi.org/10.5194/gmd-11-3481-2018, 2018.

Hanasaki, N., Matsuda, H., Fujiwara, M., Hirabayashi, Y., Seto, S., Kanae, S., and Oki, T.: Toward hyper-resolution global hydrological models including human activities: application to Kyushu island, Japan, Hydrology and Earth System Sciences, 26, 1953–1975, https://doi.org/10.5194/hess-26-1953-2022, 2022.

Hansen, B. B., Grøtan, V., Aanes, R., Sæther, B.-E., Stien, A., Fuglei, E., Ims, R. A., Yoccoz, N. G., and Pedersen, Å. Ø.: Climate Events Synchronize the Dynamics of a Resident Vertebrate Community in the High Arctic, Science, 339, 313–315, https://doi.org/10.1126/science.1226766, 2013.

Hattermann, F. F., Krysanova, V., Gosling, S. N., Dankers, R., Daggupati, P., Donnelly, C., Flörke, M., Huang, S., Motovilov, Y., Buda, S., Yang, T., Müller, C., Leng, G., Tang, Q., Portmann, F. T., Hagemann, S., Gerten, D., Wada, Y., Masaki, Y., Alemayehu, T., Satoh, Y., and Samaniego, L.: Cross-scale intercomparison of climate change impacts simulated by regional and global hydrological models in eleven large river basins, Climatic Change, 141, 561–576, https://doi.org/10.1007/s10584-016-1829-4, 2017.

Hattermann, F. F., Vetter, T., Breuer, L., Su, B., Daggupati, P., Donnelly, C., Fekete, B., Flörke, F., Gosling, S. N., P Hoffmann, Liersch, S., Masaki, Y., Motovilov, Y., Müller, C., Samaniego, L., Stacke, T., Wada, Y., Yang, T., and Krysnaova, V.: Sources of uncertainty in hydrological climate impact assessment: a cross-scale study, Environ. Res. Lett., 13, 015006, https://doi.org/10.1088/1748-9326/aa9938, 2018.

https://doi.org/10.5194/egusphere-2024-3170
Preprint. Discussion started: 22 November 2024

Heginbottom, J. A., Dubreuil, M. A., and Harker, P. A.: Canada—permafrost, National Atlas of Canada, National Atlas Information Service, Natural Resources Canada, MCR, 4177, 1995.

Heinicke, S., Volkholz, J., Schewe, J., Gosling, S. N., Schmied, H. M., Zimmermann, S., Mengel, M., Sauer, I. J., Burek, P., Chang, J., Kou-Giesbrecht, S., Grillakis, M., Guillaumot, L., Hanasaki, N., Koutroulis, A., Otta, K., Qi, W., Satoh, Y., Stacke, T., Yokohata, T., and Frieler, K.: Global hydrological models continue to overestimate river discharge, Environ. Res. Lett., 19, 074005, https://doi.org/10.1088/1748-9326/ad52b0, 2024.

Hosking, J. R. M. and Wallis, J. R.: Some statistics useful in regional frequency analysis, Water Resources Research, 29, 271–281, https://doi.org/10.1029/92WR01980, 1993.

Huang, S., Kumar, R., Flörke, M., Yang, T., Hundecha, Y., Kraft, P., Gao, C., Gelfan, A., Liersch, S., Lobanova, A., Strauch, M., van Ogtrop, F., Reinhardt, J., Haberlandt, U., and Krysanova, V.: Evaluation of an ensemble of regional hydrological models in 12 large-scale river basins worldwide, Climatic Change, 141, 381–397, https://doi.org/10.1007/s10584-016-1841-8, 2017.

van Jaarsveld, B., Wanders, N., Sutanudjaja, E. H., Hoch, J., Droppers, B., Janzing, J., van Beek, R. L. P. H., and Bierkens, M. F. P.: A first attempt to model global hydrology at hyper-resolution, EGUsphere, 1–32, https://doi.org/10.5194/egusphere-2024-1025, 2024.

Hole-filled seamless SRTM data V4 583: https://srtm.csi.cgiar.org/, last access: 17 July 2024.

Klein Goldewijk, K., Beusen, A., Doelman, J., and Stehfest, E.: Anthropogenic land use estimates for the Holocene – HYDE 3.2, Earth System Science Data, 9, 927–953, https://doi.org/10.5194/essd-9-927-2017, 2017.

Krysanova, V., Zaherpour, J., Didovets, I., Gosling, S. N., Gerten, D., Hanasaki, N., Müller Schmied, H., Pokhrel, Y., Satoh, Y., Tang, Q., and Wada, Y.: How evaluation of global hydrological models can help to improve credibility of river discharge projections under climate change, Climatic Change, 163, 1353–1377, https://doi.org/10.1007/s10584-020-02840-0, 2020.

Latifovic, R., Homer, C., Ressl, R., Pouliot, D., Hossain, S. N., Colditz, R. R., Olthof, I., Giri, C. P., and Victoria, A.: North American land change monitoring system, Remote sensing of land use and land cover: principles and applications, 303–324, 2012.

Liang, X., Lettenmaier, D. P., Wood, E. F., and Burges, S. J.: A simple hydrologically based model of land surface water and energy fluxes for general circulation models, J. Geophys. Res., 99, 14415–14428, https://doi.org/10.1029/94JD00483, 1994.

Liang, X., Wood, E. F., and Lettenmaier, D. P.: Surface soil moisture parameterization of the VIC-2L model: Evaluation and modification, Global and Planetary Change, 13, 195–206, https://doi.org/10.1016/0921-8181(95)00046-1, 1996.

Lohmann, D., Raschke, E., Nijssen, B., and Lettenmaier, D. P.: Regional scale hydrology: I. Formulation of the VIC-2L model coupled to a routing model, Hydrological Sciences Journal, 43, 131–141, https://doi.org/10.1080/02626669809492107, 1998.

Mahony, C. R., Wang, T., Hamann, A., and Cannon, A. J.: A global climate model ensemble for downscaled monthly climate normals over North America, International Journal of Climatology, n/a, https://doi.org/10.1002/joc.7566, 2022.

Meyer, J., Kohn, I., Stahl, K., Hakala, K., Seibert, J., and Cannon, A. J.: Effects of univariate and multivariate bias correction on hydrological impact projections in alpine catchments, Hydrology and Earth System Sciences, 23, 1339–1354, https://doi.org/10.5194/hess-23-1339-2019, 2019.

Molnau, M. and Bissell, V. C.: A continuous frozen ground index for flood forecasting, in: Proceedings 51st Annual Meeting Western Snow Conference, 109–119, 1983.

Nash, J. E. and Sutcliffe, J. V.: River flow forecasting through conceptual models part I — A discussion of principles, Journal of Hydrology, 10, 282–290, https://doi.org/10.1016/0022-1694(70)90255-6, 1970.

Pitié, F., Kokaram, A. C., and Dahyot, R.: Automated colour grading using colour distribution transfer, Computer Vision and Image Understanding, 107, 123–137, 2007.

Pokhrel, Y., Felfelani, F., Satoh, Y., Boulange, J., Burek, P., Gädeke, A., Gerten, D., Gosling, S. N., Grillakis, M., Gudmundsson, L., Hanasaki, N., Kim, H., Koutroulis, A., Liu, J., Papadimitriou, L., Schewe, J., Müller Schmied, H., Stacke, T., Telteu, C.-E.,

https://doi.org/10.5194/egusphere-2024-3170
Preprint. Discussion started: 22 November 2024

Thiery, W., Veldkamp, T., Zhao, F., and Wada, Y.: Global terrestrial water storage and drought severity under climate change, Nature Climate Change, 1–8, https://doi.org/10.1038/s41558-020-00972-w, 2021.

Satoh, Y., Yoshimura, K., Pokhrel, Y., Kim, H., Shiogama, H., Yokohata, T., Hanasaki, N., Wada, Y., Burek, P., Byers, E., Schmied, H. M., Gerten, D., Ostberg, S., Gosling, S. N., Boulange, J. E. S., and Oki, T.: The timing of unprecedented hydrological drought under climate change, Nat Commun, 13, 3287, https://doi.org/10.1038/s41467-022-30729-2, 2022.

Schnorbus, M., Werner, A., and Bennett, K.: Impacts of climate change in three hydrologic regimes in British Columbia, Canada, Hydrological Processes, 28, 1170–1189, https://doi.org/10.1002/hyp.9661, 2014.

Shrestha, R. R. and Rode, M.: Multi-objective calibration and fuzzy preference selection of a distributed hydrological model, Environ. Modell. Softw., 23, 1384–1395, https://doi.org/10.1016/j.envsoft.2008.04.001, 2008.

Shrestha, R. R., Schnorbus, M. A., and Peters, D. L.: Assessment of a hydrologic model's reliability in simulating flow regime alterations in a changing climate, Hydrol. Process., 30, 2628–2643, https://doi.org/10.1002/hyp.10812, 2016.

Shrestha, R. R., Cannon, A. J., Schnorbus, M. A., and Alford, H.: Climatic Controls on Future Hydrologic Changes in a Subarctic River Basin in Canada, J. Hydrometeor., 20, 1757–1778, https://doi.org/10.1175/JHM-D-18-0262.1, 2019.

Shrestha, R. R., Pesklevits, J., Yang, D., Peters, D. L., and Dibike, Y. B.: Climatic Controls on Mean and Extreme Streamflow Changes Across the Permafrost Region of Canada, Water, 13, 626, https://doi.org/10.3390/w13050626, 2021.

Shrestha, R. R., Dibike, Y. B., and Bonsal, B. R.: Snowpack driven streamflow predictability under future climate: contrasting changes across two western Canadian river basins, Journal of Hydrometeorology, 1, https://doi.org/10.1175/JHM-D-21-0214.1, 2022.

Shuttleworth, W. J.: Evaporation, in: Handbook of Hydrology, McGraw-Hill, Inc., New York, 4.1-4.53, 1993.

Smith, C. J., Kramer, R. J., Myhre, G., Alterskjær, K., Collins, W., Sima, A., Boucher, O., Dufresne, J.-L., Nabat, P., Michou, M., Yukimoto, S., Cole, J., Paynter, D., Shiogama, H., O'Connor, F. M., Robertson, E., Wiltshire, A., Andrews, T., Hannay, C., Miller, R., Nazarenko, L., Kirkevåg, A., Olivié, D., Fiedler, S., Lewinschal, A., Mackallah, C., Dix, M., Pincus, R., and Forster, P. M.: Effective radiative forcing and adjustments in CMIP6 models, Atmospheric Chemistry and Physics, 20, 9591–9618, https://doi.org/10.5194/acp-20-9591-2020, 2020.

Szeto, K. K., Tran, H., MacKay, M. D., Crawford, R., and Stewart, R. E.: The MAGS Water and Energy Budget Study, Journal of Hydrometeorology, 9, 96–115, https://doi.org/10.1175/2007JHM810.1, 2008.

Telteu, C.-E., Müller Schmied, H., Thiery, W., Leng, G., Burek, P., Liu, X., Boulange, J. E. S., Andersen, L. S., Grillakis, M., Gosling, S. N., Satoh, Y., Rakovec, O., Stacke, T., Chang, J., Wanders, N., Shah, H. L., Trautmann, T., Mao, G., Hanasaki, N., Koutroulis, A., Pokhrel, Y., Samaniego, L., Wada, Y., Mishra, V., Liu, J., Döll, P., Zhao, F., Gädeke, A., Rabin, S. S., and Herz, F.: Understanding each other's models: an introduction and a standard representation of 16 global water models to support intercomparison, improvement, and communication, Geoscientific Model Development, 14, 3843–3878, https://doi.org/10.5194/gmd-14-3843-2021, 2021.

Thornton, P. E. and Running, S. W.: An improved algorithm for estimating incident daily solar radiation from measurements of temperature, humidity, and precipitation, Agricultural and Forest Meteorology, 93, 211–228, 1999.

Thornton, P. E., Hasenauer, H., and White, M. A.: Simultaneous estimation of daily solar radiation and humidity from observed temperature and precipitation: an application over complex terrain in Austria, Agricultural and Forest Meteorology, 104, 255–271, https://doi.org/10.1016/S0168-1923(00)00170-2, 2000.

Veldkamp, T. I. E., Zhao, F., Ward, P. J., Moel, H. de, Aerts, J. C. J. H., Schmied, H. M., Portmann, F. T., Masaki, Y., Pokhrel, Y., Liu, X., Satoh, Y., Gerten, D., Gosling, S. N., Zaherpour, J., and Wada, Y.: Human impact parameterizations in global hydrological models improve estimates of monthly discharges and hydrological extremes: a multi-model validation study, Environ. Res. Lett., 13, 055008, https://doi.org/10.1088/1748-9326/aab96f, 2018.

Warden, J. W., Rezvani, R., Najafi, M. R., and Shrestha, R. R.: Projections of rain-on-snow events in a sub-arctic river basin under 1.5°C–4°C global warming, Hydrological Processes, 38, e15250, https://doi.org/10.1002/hyp.15250, 2024.

https://doi.org/10.5194/egusphere-2024-3170
Preprint. Discussion started: 22 November 2024

Werner, A. T., Schnorbus, M. A., Shrestha, R. R., Cannon, A. J., Zwiers, F. W., Dayon, G., and Anslow, F.: A long-term, temporally consistent, gridded daily meteorological dataset for northwestern North America, Scientific Data, 6, 180299, https://doi.org/10.1038/sdata.2018.299, 2019.

Woo, M.-K. and Thorne, R.: Snowmelt contribution to discharge from a large mountainous catchment in subarctic Canada, Hydrological Processes, 20, 2129–2139, https://doi.org/10.1002/hyp.6205, 2006.

Zaherpour, J., Gosling, S. N., Mount, N., Schmied, H. M., Veldkamp, T. I. E., Dankers, R., Eisner, S., Gerten, D., Gudmundsson, L., Haddeland, I., Hanasaki, N., Kim, H., Leng, G., Liu, J., Masaki, Y., Oki, T., Pokhrel, Y., Satoh, Y., Schewe, J., and Wada, Y.: Worldwide evaluation of mean and extreme runoff from six global-scale hydrological models that account for human impacts, Environ. Res. Lett., 13, 065015, https://doi.org/10.1088/1748-9326/aac547, 2018.

Zhao, R. J. and Liu, X. R.: The Xinanjiang model, in: Computer Models of Watershed Hydrology, 215–232, 1995.

Zscheischler, J., Fischer, E. M., and Lange, S.: The effect of bias adjustment on impact modeling, Earth System Dynamics Discussions, 1–17, https://doi.org/10.5194/esd-2018-68, 2018.